Applied Catalysis B: Environmental 90 (2009) 295–306

Contents lists available at ScienceDirect

Applied Catalysis B: Environmental

journal homepage: www.elsevier.com/locate/apcatb

Kinetic modeling of the total oxidation of propane over anatase and vanadia sputter deposited catalysts

Philippe M. Heynderickx [a], Joris W. Thybaut [a,*], Hilde Poelman [b], Dirk Poelman [b], Guy B. Marin [a]

[a] Laboratory for Chemical Technology, Department of Chemical Engineering, Ghent University, Ghent, B-9000, Belgium
[b] Department of Solid State Sciences, LumiLab, Ghent University, Ghent, B-9000, Belgium

ARTICLE INFO

Article history:
Received 2 December 2008
Received in revised form 13 March 2009
Accepted 16 March 2009
Available online 25 March 2009

Keywords:
Propane total oxidation
Sputter deposited catalysts
Kinetic modeling
Mars–van Krevelen
Compensation effect

ABSTRACT

Using an innovative magnetron sputter deposition technique, a set of titania (anatase), vanadia and vanadia–titania (anatase) based catalysts on porous SiO_2 and non-porous SiO_2–ZrO_2 supports is prepared. These catalysts are tested for propane total oxidation at atmospheric pressure, a constant oxygen inlet partial pressure of 28.4 kPa and temperatures from 733 to 773 K. The inlet ratio of oxygen and propane is varied between 7.7 and 85.3 mol mol^{-1}. A longer TiO_x sputter deposition time has a beneficial effect on the propane total oxidation turnover frequency (TOF). Furthermore, the use of a porous support results in higher TOF. Starting from eleven possible rate equations, the one corresponding to a Mars–van Krevelen (MVK) mechanism, involving one active site in the reduction and reoxidation step, is globally the most significant. A pronounced compensation effect is observed for the rate coefficients of the reoxidation and reduction steps.

1. Introduction

Volatile organic compounds (VOC) exhibit a significant vapor pressure at ambient conditions. Emissions from both stationary and non-stationary sources are subjected to a strict legislation due to increasing environmental awareness. Oxidation on heterogeneous transition metal oxide catalysts offers the advantage that VOC can be removed from industrial effluent gas streams even if they are present in very low concentrations [1]. For stationary VOC sources, transition metal oxides are preferred to noble metals, because of their lower cost, possible higher thermal stability and better resistance to poisoning [2]. Recently, an innovative magnetron sputter deposition technique was applied for the production of metal oxide catalysts [3,4]. The resulting catalysts were shown to be active in oxidation reactions, such as the oxidative dehydrogenation of propane and isobutane.

The present paper describes the total oxidation of propane as a model reaction over ten sputter deposited catalysts by means of steady-state experiments in a conventional plug flow reactor. Kinetic analysis of the experimental data gives a better insight into the effect of the deposition procedure on the oxidation rate.

Abbreviations: BET, Brunauer–Emmett–Teller; ER, Eley–Rideal; ICP, inductively coupled plasma; LH, Langmuir–Hinshelwood; MVK, Mars–van Krevelen; N, non-porous; P, porous; TOF, turnover frequency; VOC, volatile organic compound.

* Corresponding author. Tel.: +32 9 264 45 19; fax: +32 9 264 49 99.
E-mail address: Joris.Thybaut@UGent.be (J.W. Thybaut).

0926-3373/$ – see front matter © 2009 Elsevier B.V. All rights reserved.
doi:10.1016/j.apcatb.2009.03.020

2. Procedures

2.1. Catalysts

In total, ten catalysts are made by means of the magnetron sputter depositing technique, using particle sizes between 250 and 400 μm. Details of this technique are reported elsewhere [4–7]. Two sputter deposited catalyst samples, Ti3-P and Ti6-P, are obtained by performing a TiO_x sputter deposition during 3 and 6 h on a porous SiO_2 support. The latter has a BET surface area of 232 m^2 g_{cat}^{-1}. A non-porous SiO_2–ZrO_2 support, denoted as N in the label, is used to obtain the sputter deposited catalyst samples Ti3-N and Ti6-N [5]. VO_x sputter deposition is performed during 11 h on bare support as well as on the two TiO_x sputter deposited samples for each of the two supports, resulting in six additional sputter deposited catalyst samples: V-P, Ti3V-P and Ti6V-P for the porous support and V-N, Ti3V-N and Ti6V-N for the non-porous support. After each sputter deposition treatment the catalyst samples are calcined at 873 K during 1 h in air.

2.2. Catalyst properties

2.2.1. Oxygen storage capacity

The catalyst's oxygen storage capacity, C_O, is determined by pulse chemisorption experiments using a Micromeritics AutoChem 2920. 300 mg of catalyst is loaded and pretreated in air during 1 h at 1073 K. Subsequently, the sample is cooled down to

Nomenclature

a_v	specific external surface area (m^{-1})
A	constant used in Eq. (4) (mol mol^{-1})
A'	constant used in Eq. (10) (mol kg_{cat}^{-1} s^{-1})
A_k	peak surface area of component k (V s)
b_c	constant used in Eq. (14) (−)
b	volumetric dilution degree (m^3 m^{-3})
B	constant used in Eq. (4) (mol kg_{cat}^{-1} s^{-1})
Bo	Bodenstein number (−)
C_i	concentration of component i (mol kg_{cat}^{-1})
d	diameter (m)
d_k	calibration factor for component k used in Eq. (3) (V s mol^{-1})
D_i	diffusion coefficient for component i (m^2 s^{-1})
E	activation energy (kJ mol^{-1})
F_i	molar flow rate of component i (mol s^{-1})
ΔH_i	adsorption enthalpy for component i (kJ mol^{-1})
$-\Delta_r H$	reaction enthalpy (kJ mol^{-1})
k	reaction coefficient (dep.)
k_g	mass transfer coefficient (m s^{-1})
K_j	adsorption equilibrium coefficient for component j (kPa^{-1})
L	catalyst bed length (m)
m_c	constant used in Eq. (14) (mmol J^{-1})
m	model number (−), partial reaction order for propane (−)
n	partial reaction order for oxygen (−)
n_i	number of carbon atoms in component i (−), reaction order of component i (−)
n_j	number of experiments on temperature level j (−)
n_k	partial reaction order towards component k
N	number of peaks before saturation, vide Eq. (1) (−)
N_C	number of carbon-containing components (−)
N_T	number of temperature levels (−)
p	pressure (kPa)
r	specific reaction rate (mol kg_{cat}^{-1} s^{-1})
R	universal gas constant (kJ mol^{-1} K^{-1})
ΔS	adsorption entropy (J mol^{-1} K^{-1})
S_m	residual sum of squares, vide Eq. (8) (mol^2 mol^{-2})
T	temperature (K)
u	velocity (m s^{-1})
V	volume (m^3)
W_{cat}	mass of catalyst (kg_{cat})
X	fractional conversion (mol mol^{-1})

Greek letters

α	heat transfer coefficient (J m^{-2} s^{-1} K^{-1})
α_s	specific surface area (m^2 g_{cat}^{-1})
ε_b	bed porosity (m^3 m^{-3})
γ	ratio of oxygen and propane partial pressures (mol mol^{-1})
φ	quantity defined in Table 6 (model MVK2)
φ'	quantity defined in Table 6 (model MVK3)
λ	heat transfer coefficient (J m^{-1} s^{-1} K^{-1})
μ	viscosity (Pa s)
θ	fraction of active sites (−)
ρ	density (kg m^{-3})

Subscripts

app	apparent
b	bulk
c	compensation
eff	effective
f	fluid
i	component i
inj	injection
iso	isokinetic
obs	observed
p	particle
s	surface
t	tube
tot	total
0	initial, superficial

Superscripts

calc	calculated
obs	observed
0	saturation
^	calculated
*	reference, surface species
′	reparametrized

773 K and a H_2 flow rate of 1.04×10^{-6} mol s^{-1} is established during 10 min. As evidenced from Table 1, the admitted amount of H_2 is at least hundred times higher than the oxygen storage capacity of the catalyst present in the sample holder. Next, oxygen pulse chemisorption is performed, in which He is used as carrier gas and changes in the effluent gas are measured with a thermal conductivity detector. The concentration of oxygen atoms consumed in a pulse chemisorption experiment after maximal reduction at 773 K is calculated from Eq. (1), where V_{inj} is the loop volume injected, A_i the peak surface area corresponding to injection i and A_N the peak surface area corresponding to the injected volume when no further oxygen chemisorption occurs (saturation). A series of injections is performed after saturation, from which an experimental standard deviation for A_N is obtained. Applying a constant injection volume V_{inj}, temperature T_{inj} and pressure p_{inj} gives then the standard deviation for the oxygen storage capacity calculated with Eq. (1), as mentioned in Table 1.

$$C_O = \frac{2}{R}\frac{p_{inj}V_{inj}}{T_{inj}}\sum_{i=1}^{N-1}\left(1-\frac{A_i}{A_N}\right) \quad (1)$$

2.2.2. Bulk chemical composition

The bulk chemical composition of the sputter deposited catalyst samples was determined by means of inductively coupled plasma (ICP) atomic emission spectrometry (IRIS Advantage system, Thermo Jarrell Ash). Acid dissolution in HNO_3, HF and $HClO_4$ was used for the sputter deposited catalysts on the non-porous support, while dissolution in HNO_3 and HF was applied when the

Table 1
Oxygen storage capacity at 773 K, C_O (mmol kg_{cat}^{-1}), calculated with Eq. (1), is reported with the corresponding experimental standard deviation, vide Section 2.2.1. p_{inj} = 101.3 kPa; T_{inj} = 384 K; $V_{inj} = 5.0 \times 10^{-7}$ m^3.

Sputter deposition	Non-porous support	Porous support
Ti3	4.60 ± 2.15	5.23 ± 1.33
Ti6	1.96 ± 0.27	4.29 ± 0.41
V	2.39 ± 0.29	21.0 ± 0.69
Ti3V	3.88 ± 0.82	16.8 ± 1.49
Ti6V	2.84 ± 0.40	11.0 ± 0.11

porous support was used. Standard deviations for the nominal bulk chemical composition are obtained from replicate experiments.

2.2.3. BET surface area

N_2 physisorption at 77 K is applied to determine the BET specific surface area using a Gemini V (Micromeritics) automated system. Before every measurement, a catalyst sample of 300 mg is degassed during 1 h under N_2 atmosphere at 573 K in a FlowPrep 060 (Micromeritics). BET values with their 95% confidence intervals are obtained by regression of the experimental data in the range $0.05 < p/p^0 < 0.30$ with the linear BET equation [8].

2.2.4. Temperature-programmed reduction (TPR)

H_2-TPR experiments are performed in order to determine the reducibility of the sputter deposited catalysts. Before the reduction measurement, the samples were calcined in air at 1073 K for 1 h and cooled to 323 K under He. TPR profiles are obtained at a heating rate of 30 K min^{-1} up to 1073 K under a flow of 0.05 mol mol^{-1} H_2 in Ar using 2.0 g of catalyst material and a total molar flow rate of 4.46×10^{-5} mol s^{-1}. The experimental conditions satisfy the criterion of Malet and Caballero [9], given by Eq. (2). β^* is the heating rate, S_0 is the initial molar amount of reducible substance and $F_{H_2,0}$ is the inlet molar flow rate of the reducing agent. This criterion guaranties the TPR profile resolution [10]. For the series of catalysts the left hand side of Eq. (2) varies from 0.09 to 0.84, and hence, the given criterion is fulfilled for all experimental TPR conditions.

$$\frac{1}{20}\frac{\beta^* S_0}{F_{H_2,0}} < 1 \tag{2}$$

2.3. Kinetic experiments

Evaluation of the catalytic activity in the total oxidation of propane is carried out in a conventional fixed-bed reactor with inner diameter of 1.4×10^{-2} m, using 4 g of catalyst, diluted with 20 g of inert. The range of investigated experimental conditions is given in Table 2. Effluent gases are analyzed on-line using a GC 8000 gas chromatograph (CE Instruments) with a thermal conductivity detector, using methane as internal standard. The carbon mole balance is closed within 5%. The only products formed are water and carbon dioxide. No partial oxidation products such as propene or carbon monoxide are detected in the reactor effluent mixture, which is in accordance with the high inlet ratio of oxygen to propane [11–13]. Before the effluent gases enter the gas chromatograph, the water is removed with a drierite column. The separation occurs on a Porapak Q column using a temperature program. In total, 282 experimental points are acquired.

Table 2
Range of experimental conditions during the steady-state total oxidation of propane over a series of sputter deposited catalysts. Helium is used as balance gas.

Process condition	SI unit	Range
$p_{C_3H_8,0}$	kPa	0.33–3.71
$p_{O_2,0}$	kPa	28.4
$\gamma_0 = y_{O_2,0} y_{C_3H_8,0}^{-1}$	mol mol^{-1}	7.7–85.3
$W_{cat} F_{C_3H_8,0}^{-1}$	kg_{cat} s mol^{-1}	492–1970
T	K	733–773
$X_{C_3H_8}$	mol mol^{-1}	0.01–0.52

The conversion of propane is calculated using the normalization method, vide Eq. (3), in which A_i and d_i represent the surface area obtained for component i in the chromatogram and the corresponding calibration factor; n_i is the number of carbon atoms in component i and N_C is the number of carbon containing components in the reactor effluent. Every analysis is performed at least three times in order to obtain an average value for the corresponding propane conversion.

$$X_{C_3H_8} = \frac{\sum_{i=1_{i\neq C_3H_8}}^{N_C} n_i A_i / d_i}{\sum_{i=1}^{N_C} n_i A_i / d_i} \tag{3}$$

Criteria for plug flow regime as well as for negligible concentration and temperature gradients on pellet and reactor scale are reported by Berger et al. [14]. The catalyst bed length is 7.9×10^{-2} m with a bed porosity of 0.41 m^3 m^{-3}. An effective diffusion coefficient of 7.5×10^{-7} m^2 s^{-1} and a tortuosity of 2.5 m m^{-1} for the porous catalysts is used. For a maximal initial specific reaction rate of 4.89×10^{-4} mol kg_{cat}^{-1} s^{-1} on sample Ti6V-P, a maximum reaction temperature of 773 K, a maximum propane conversion of 0.52 mol mol^{-1} and a maximum activation energy for propane combustion of 134.7 kJ mol^{-1} these criteria are verified. Table 3 shows that according to these criteria plug flow regime is established and concentration and temperature gradients on pellet as well as on reactor scale can be neglected.

Table 3
Overview of the criteria for plug flow regime and concentration and temperature gradients [14,22,53–55].

	Criterion	Mathematical form ($A < B$)	A	B
1	Assumption plug flow regime	$8.0 < \frac{d_t}{d_p}$	8.0	53.3
2	Assumption plug flow regime	$\frac{8}{Bo} m \ln\frac{1}{1-X_{C_3H_8}} < \frac{L}{d_p}$	42.1	210.6
3	Dilution of the catalyst bed	$\left(\frac{b}{1-b}\right)\frac{X_{C_3H_8} d_p}{2L} < 0.05$	2.5×10^{-3}	0.05
4	Pressure drop	$\frac{0.15(1-\varepsilon_b)^2 \mu_f u_0 L}{\varepsilon_b^3 {d_p}^2} + \frac{0.00175(1-\varepsilon_b)\rho_f u_0^2 L}{\varepsilon_b^3 d_p} < \frac{0.2\, p_{tot}}{m}$	0.2	20.5
5	External mass transfer limitation	$\frac{r_{obs}}{k_g a_v C_{C_3H_8,b}} < \frac{0.05}{m}$	7.5×10^{-5}	0.05
6	Internal mass transfer limitation	$\frac{r_{obs}}{D_{C_3H_8,eff} C_{C_3H_8,b}}\left(\frac{d_p}{6}\right)^2 < \frac{1}{12m}$	0.004	0.083
7	External heat transfer limitation	$\frac{r_{obs}(-\Delta_r H) d_p}{6\alpha} < \frac{0.05 R T_f^2}{E}$	0.05	1.84
8	Internal heat transfer limitation	$\frac{r_{obs}(-\Delta_r H) d_p^2}{60\lambda_p} < \frac{0.05 R T_f^2}{E}$	1.4×10^{-3}	1.84
9	Radial heat transfer limitation	$\frac{r_{obs}(-\Delta_r H)(1-\varepsilon_b)(1-b) d_t^2}{6\alpha} < \frac{0.05 R T_w^2}{E}$	0.40	1.84

2.4. Apparent activation energies and initial turnover frequencies

In order to estimate initial specific reaction rates, Eq. (4) is regressed to the experimental propane conversion vs. space time curves [15]:

$$X_{C_3H_8} = A\left(1 - \exp\left(-B\frac{W_{cat}}{F_{C_3H_8,0}}\right)\right) \quad (4)$$

Since concentration and temperature gradients can be neglected as well as the conditions for plug flow regime are fulfilled, vide Section 2.3, the continuity equation for propane can be written as Eq. (5):

$$\frac{dX_{C_3H_8}}{d(W_{cat}/F_{C_3H_8,0})} = r \quad (5)$$

The initial specific reaction rate is then obtained as the first derivative of Eq. (4) with respect to the space time at zero space time. From these observed initial specific reaction rates at different temperature levels apparent activation energies can be determined when a simple power law kinetic model, Eq. (6), is proposed to describe the experimental data.

$$r_0 = k\, p_{C_3H_8,0}^m\, p_{O_2,0}^n \quad (6)$$

Taking the logarithm of Eq. (6) results in Eq. (7), which allows to estimate the apparent activation energy for the propane total oxidation, E_{app}^{obs}, by regression of the initial specific reaction rates at given propane and oxygen inlet partial pressures. For all catalyst samples, the multiple correlation coefficient is at least 0.987.

$$\ln(r_0) = m\ln(p_{C_3H_8,0}) + n\ln(p_{O_2,0}) + \ln(k_0) - \frac{E_{app}^{obs}}{RT} \quad (7)$$

Dividing the initial reaction rates r_0 by C_O, vide Table 1 and Section 3.1, yields the corresponding initial TOF.

2.5. Kinetic analysis of experimental data: modeling based on elementary steps

In this section the mathematical expression of the specific reaction rate r is based on mechanistic modeling. A list of eleven possible kinetic models is proposed in Table 6. Based on a well-considered strategy the best model is selected. This procedure, albeit for a lower number of kinetic models, has been applied successfully before [16–19].

Four Langmuir–Hinshelwood (LH) mechanisms are considered, accounting for the competitive adsorption of propane and oxygen with the surface reaction as rate-determining step. C–H bond activation in saturated hydrocarbons is the crucial first step in the combustion of these components and this step occurs on the catalyst surface [20]. The distinctive features between the considered LH models are the molecular, models LH1 and LH2, or dissociative, models LH3 and LH4, chemisorption of oxygen and the number of oxygen surface species consumed in the rate-determining step, i.e., one, models LH1 and LH3, or two, models LH2 and LH4. Given the variation in propane inlet partial pressures, a clear discrimination between the kinetic models with different propane partial pressure dependence, e.g. LH1 and LH2, is possible. Despite the constant oxygen inlet partial pressure, discrimination between models with the same propane partial pressure dependence, e.g. LH2 and LH4, is also possible, albeit less clear, because of the integral character of the measurements, vide Eq. (5), and, hence, the variation in oxygen partial pressure with the axial position in the catalyst bed.

The list of possible models is extended with four Eley–Rideal (ER) models, featuring oxygen chemisorption and reaction with propane from the gas phase. The fact that oxygen is assumed to adsorb can be justified by the high inlet oxygen partial pressure, compared to the propane inlet partial pressure, vide Table 2. Models ER1 and ER2 describe the associative oxygen adsorption and one or two adsorbed oxygen species are used in the reaction with propane from the gas phase respectively. Models ER3 and ER4 consider the reaction of gas phase propane with one or two dissociatively adsorbed species respectively. Finally, three Mars–van Krevelen (MVK) models are added to the list in Table 6. Model MVK1 corresponds with a reduction step in which propane reacts with a single oxidized site and with a reoxidation step by gas phase oxygen, involving a single reduced surface site. The factor '5' in the denominator of the corresponding rate equation originates from the number of oxygen molecules needed in the total oxidation of one propane molecule [21]. It is assumed in model MVK2 that the reoxidation involves gas phase oxygen and two reduced surface sites. Model MVK3 expresses that the reduction uses two oxidized sites from the catalyst surface.

The ultimate goal in a kinetic analysis is the non-isothermal parameter regression of all experimental data simultaneously, in which the objective function for every model m, Eq. (8), is minimized with a Levenberg–Marquardt algorithm [22]. The first step in this respect is an isothermal analysis in which the objective function, Eq. (9), corresponding to model m is minimized at every temperature level j. In this paper, the experimental propane conversion, as obtained from Eq. (3), is used as response. Both Eqs. (8) and (9) are based upon the assumption that the experimental errors are normally distributed with a zero mean.

$$S_m = \sum_{j=1}^{N_T}\sum_{i=1}^{n_j}(X_i - \hat{X}_{i,m})^2 \rightarrow \text{minimum} \quad (8)$$

$$S_{m,j} = \sum_{i=1}^{n_j}(X_i - \hat{X}_{i,m})^2 \rightarrow \text{minimum} \quad (9)$$

For non-isothermal regression analysis, reaction rate coefficients and adsorption equilibrium coefficients are reparametrized as given in Eqs. (10) and (11). By this means, binary correlation between pre-exponential factors and activation energies is reduced and the computational effort for the minimization of the objective function is diminished [23,24]. The binary correlation coefficient is a number that summarizes the direction and degree of linear correlations between two variables. The absolute value of this coefficient should exceed 0.95 before any correlation between the two corresponding parameters is considered significant. The reference temperature T^* is a number-averaged value over the applied temperature range.

$$k_i = \exp\left[A_i' - \frac{E_i}{R}\left(\frac{1}{T} - \frac{1}{T^*}\right)\right] \quad (10)$$

$$K_j = \exp\left[\frac{\Delta S_j'}{R} + \frac{\Delta H_j}{R}\left(\frac{1}{T} - \frac{1}{T^*}\right)\right] \quad (11)$$

The parameter estimates are tested for their statistical significance, based on their individual t values. The statistical significance of the global regression is expressed by means of the F test [22,24]. The performance of a set of kinetic models can be evaluated using the so-called likelihood ratio [22]. The latter is defined as the ratio of the joint probability density functions evaluated at the maximum likelihood estimate. It is used as a selection criterion between rival kinetic models.

Selection between the models, proposed in Table 6, is performed using the experimental data set acquired on the catalyst with the highest propane conversion, namely Ti6V-P. The resulting model, MVK1, is successfully used to describe the experimental data obtained on the other nine catalyst samples. A fit at least as good as on the data on the Ti6V-P catalyst sample is obtained, vide Section 6.

Table 4
Bulk compositions with standard deviations. BET surface areas α_s with their 95% confidence intervals obtained from regression of the linear BET equation [8].

Sputter deposition	Non-porous support		Porous support	
	C_{Ti} or C_V (mmol kg_{cat}^{-1})	α_s (m^2 g_{cat}^{-1})	C_{Ti} or C_V (mmol kg_{cat}^{-1})	α_s (m^2 g_{cat}^{-1})
Ti3	5.17 ± 0.19	0.005[b]	18.9 ± 0.50	224.6 ± 3.5
Ti6	11.9 ± 0.59	0.005[b]	54.9 ± 1.13	218.6 ± 3.5
V	1.63 ± 0.01	0.005[b]	28.6 ± 1.49	207.6 ± 3.2
Ti3V	3.10 ± 0.12[a]	0.005[b]	22.5 ± 1.45[a]	216.0 ± 3.4
Ti6V	2.50 ± 0.01[a]	0.005[b]	17.4 ± 1.99[a]	142.0 ± 2.1

[a] V content.
[b] Measured value is below detection limit; value, reported in [5], is taken.

3. Experimental results

3.1. Catalyst characterization

The values for the oxygen storage capacity of the sputter deposited catalysts at 773 K are reported in Table 1. An unexpected reducibility of TiO_x sputter deposited catalysts is observed. An explanation can be found in the type of oxygen present on the catalyst, vide Section 3.2. As expected, the oxygen storage capacity is significantly lower on the catalysts with the non-porous support than on those with the porous support. For an identical sputter deposition treatment, the difference in oxygen storage capacity for the vanadia sputtered catalysts amounts up to one order of magnitude. Additionally, for the series V-P, Ti3V-P and Ti6V-P an approximately linear decrease is observed, while an approximately constant value is reported on the non-porous support. The latter observation can be attributed to the fact that, the geometrical surface area is not significantly influenced by the first deposition, and hence, the second sputter deposition experiences always approximately the same accessible area. For the porous support, the TiO_x sputter deposition gives a close to constant oxygen storage capacity for the two deposition times, which indicates that also in this case the accessible area is not changing appreciably. A linear decrease in oxygen storage capacity with the TiO_x sputter deposition time is observed for the VO_x sputtered catalysts on the porous support. This can be at least partially, if not fully, ascribed to the progressive blocking of the pores by the VO_x sputter deposition. The blocking of the pores is also evidenced by the BET surface area measurements and the significantly lower value obtained for the sample with the highest Ti and V loading, i.e., Ti6V-P, vide Table 4.

ICP results are given in Table 4: for the Ti3 and Ti6 sputter depositions the bulk amount of Ti is reported and for the V, Ti3V and Ti6V sputter depositions the bulk amount of V is mentioned. For the former series, a double sputter deposition time yields as expected a double amount of Ti. For the VO_x sputter deposition series, a linear relation is observed between the oxygen storage capacity, determined by two pulse chemisorption, and the bulk amount of V in the catalyst samples, vide Fig. 1. This indicates that the H_2 reduction pretreatment before the O_2 pulse chemisorption, vide Section 2.2.1, involves not only the surface oxygen atoms, but also the lattice oxygen atoms, and hence, the value for the number of oxygen moles obtained from O_2 pulse chemisorption experiments is a reliable value for the total available oxygen concentration in the sputter deposited catalyst samples.

When the reaction temperature reaches the Tammann temperature, defined as half of the melting temperature, the bulk atoms are assumed to have enough energy to diffuse from the bulk to the catalyst surface and vice versa [25,26]. The Tammann temperature of V_2O_5 is 482 K, which is below the range of applied reaction temperatures, and hence, oxygen diffusion from the bulk towards the surface and vice versa is quite acceptable. According to literature [27,28], the four steps in the reduction process of V_2O_5 can be described as: $V_2O_5 \rightarrow V_6O_{13} \rightarrow VO_2 \rightarrow V_nO_{2n-1} \rightarrow V_2O_3$, with $4 < n < 8$. Using the experimental data from Fig. 1, the final oxidation state at 773 K is given by $VO_{1.78}$, corresponding to $n = 4.45$.

The measured specific surface area for the sputter deposited catalysts on the non-porous support is not significantly different from zero, and therefore, the geometrical surface area of 5.0×10^{-3} m^2 g_{cat}^{-1} is used [5], vide Table 4. When the porous support is used, a TiO_x sputter deposition of three or six hours apparently does not significantly influence the specific surface area. On the other hand, when VO_x is sputter deposited after a first TiO_x sputter deposition of 6 h, a significant decrease in specific surface area is observed for Ti6V-P.

There are three possible measures for the total active site concentration: (i) the active metal content from ICP measurements; (ii) the number of H_2 moles consumed in TPR experiments or (iii) the total oxygen concentration C_O from reduction/reoxidation pulse chemisorption experiments at a given temperature, i.e., the oxygen storage capacity.

In literature, a VO_x sputter deposition of 5.5 h results in a theoretical number of 22 monolayers [5]. In this study, VO_x is sputter deposited for 11 h, and hence, it can be concluded that the active metal content cannot be considered as representative for the total active site concentration accessible at the catalyst surface. Although the amount of hydrogen consumed in a TPR experiment can in principle be used as a measure of the total active site concentration [29], the TPR spectra obtained in this work only

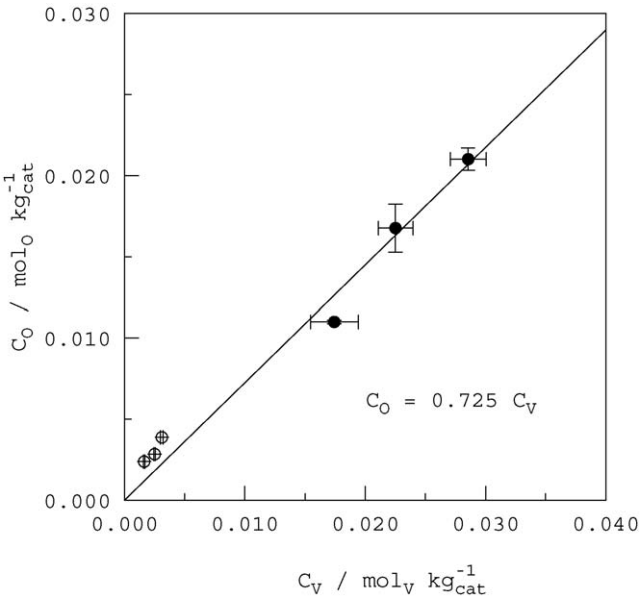

Fig. 1. Concentration of chemisorbed oxygen C_O vs. C_V bulk amount in the VO_x sputter deposited series. (●) Porous support; (○) non-porous support. Error bars represent the standard deviations for C_O and C_V, reported in Table 1 and Table 4.

allowed a qualitative interpretation in terms of reducibility rather than a quantification of the total concentration of active sites. The low active metal loadings, i.e., below 0.3 wt.%, are believed to be at the origin of this phenomenon, vide Table 4. On the other hand, the oxygen storage capacity can be accurately measured on the catalysts used in this work. Therefore, the latter value is used as a measure for the total concentration of active sites. Although this value is most likely not limited to oxygen present at the catalyst surface but also accounts for some sub-surface oxygen, it is expected to provide a sound basis for comparison assuming that the oxygen storage capacity is at least proportional if not representative for the amount of oxygen that can participate in the reaction [30–34]. In this work, the oxygen storage capacity is determined at 773 K, i.e., the highest temperature used in the experimental program.

3.2. Effects of reaction conditions

The effect of the reaction temperature on the propane conversion is given in Fig. 2. Light-off curves for the series V, Ti3V and Ti6V shift towards higher temperatures when non-porous instead of porous support is used, vide Fig. 2a, which can be related to the higher concentration of active sites upon the latter, vide Section 3.1. Whereas the value for the propane conversion obeys the order V ≈ Ti3V < Ti6V when non-porous support is used, a somewhat inconsequent order is observed on the porous support: Ti3V < V < Ti6V. When the concentration of active sites, as determined in Section 2.2.1, is taken into consideration, the same order of activity, based on TOF, is obtained: V ≈ Ti3V < Ti6V, indicating the positive effect of the first TiO_x sputter deposition on the activity per active site. Fig. 2b displays the propane conversion vs. reaction temperature for the TiO_x sputter deposited samples. Some activity is observed on the TiO_x sputtered catalysts, i.e., Ti3-N, Ti6-N, Ti3-P and Ti6-P. There is no appreciable effect of the Ti sputtering time at the operating conditions considered on the non-porous catalysts, while the longer sputtering time on the porous support leads to a small increase in the conversion. Moreover, the activity of the porous catalysts is slightly higher than that of the non-porous catalysts which can be directly related to the higher accessible surface of the former. This is also reflected in the oxygen storage capacities obtained for these catalysts, vide Table 1.

The activity of Ti3-P and Ti6-P, i.e., the samples without V, is somewhat unexpected, but the occurrence of O_2^-, O_2^{2-} and O^- species, which are known to be active in total oxidation reactions [35–37], has been previously reported on TiO_2 catalysts [38]. Therefore, the kinetics obtained on the TiO_x sputtered catalysts with the higher activity, Ti3-P and Ti6-P, are examined in some more detail, vide Fig. 3: the propane conversion as a function of the propane inlet partial pressure on the Ti3-P and Ti6-P samples is displayed at three temperature levels. Within the range of applied experimental conditions, vide Table 2, the propane conversion increases with the propane inlet partial pressure before reaching a constant value. At every temperature level this constant value is higher on Ti6-P than on Ti3-P and it is only reached at higher propane inlet partial pressures. Interpreting these phenomena according to a LH mechanism, higher propane partial reaction orders and, hence, lower propane surface concentrations, are expected on the Ti6-P catalyst compared to the Ti3-P. According to a MVK mechanism, these observations are explained by means of the ratio of the rate coefficients for reduction and reoxidation, vide Section 6.

4. Initial turnover frequency analysis

Fig. 4 depicts the effect of the support on the observed initial TOF at $p_{C_3H_8,0} = 1.16$ kPa and $p_{O_2,0} = 28.4$ kPa for the three applied reaction temperatures. For the Ti3 samples, the initial TOF over the porous and non-porous support is approximately equal. When the Ti6 sputter deposition is examined, however, the activity per site is significantly lower on the porous support. A second observation is that the VO_x sputter deposition on the catalysts with the porous support leads to higher TOF values than on the catalysts with the non-porous support.

The observed apparent activation energies on the TiO_x sputter deposition catalyst samples, reported in Table 5, are lowered when the sputter deposition time is doubled: for the non-porous support the apparent activation energy is lowered with 19 kJ mol^{-1}. In a similar way, a decrease of 15 kJ mol^{-1} is observed for the porous

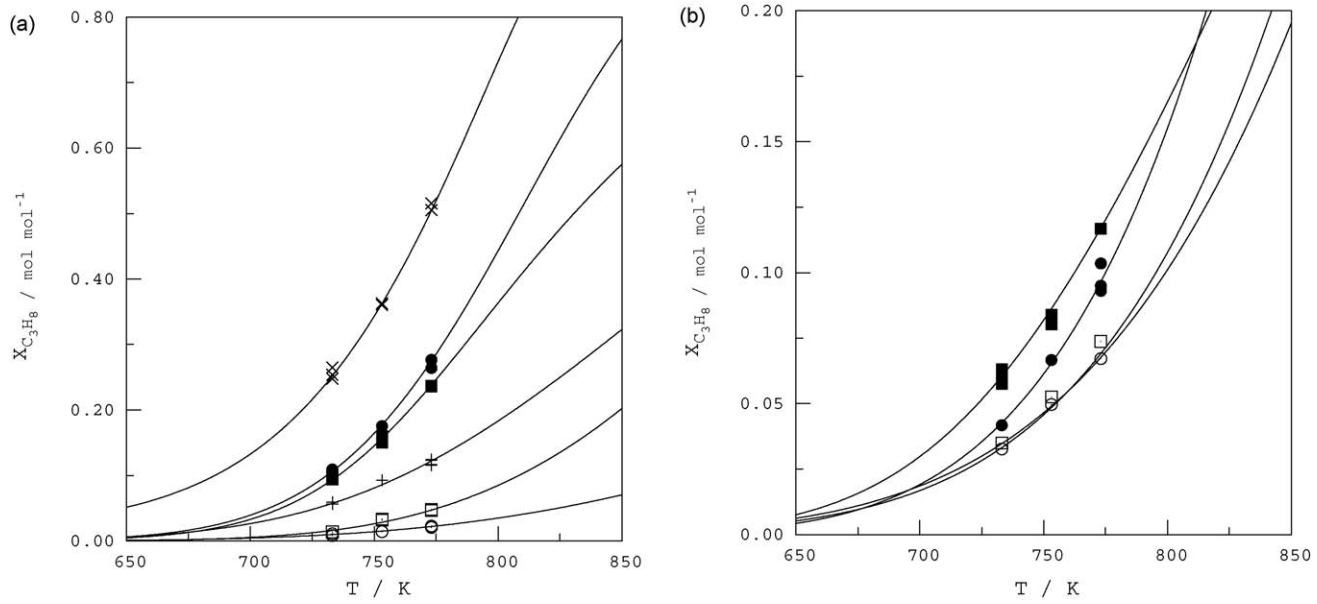

Fig. 2. Propane conversion vs. reaction temperature for (a) (○) V-N; (□) Ti3V-N; (+) Ti6V-N; (●) V-P; (■) Ti3V-P; (×) Ti6V-P and (b) (○) Ti3-N; (□) Ti6-N; (●) Ti3-P; (■) Ti6-P. Full lines are obtained with model MVK1, reported in Table 6, and corresponding kinetic parameter values from Table 8 at $p_{C_3H_8,0} = 1.16$ kPa, $p_{O_2,0} = 28.4$ kPa and $W_{cat}F_{C_3H_8,0}^{-1} = 1970\ kg_{cat}\ s\ mol^{-1}$.

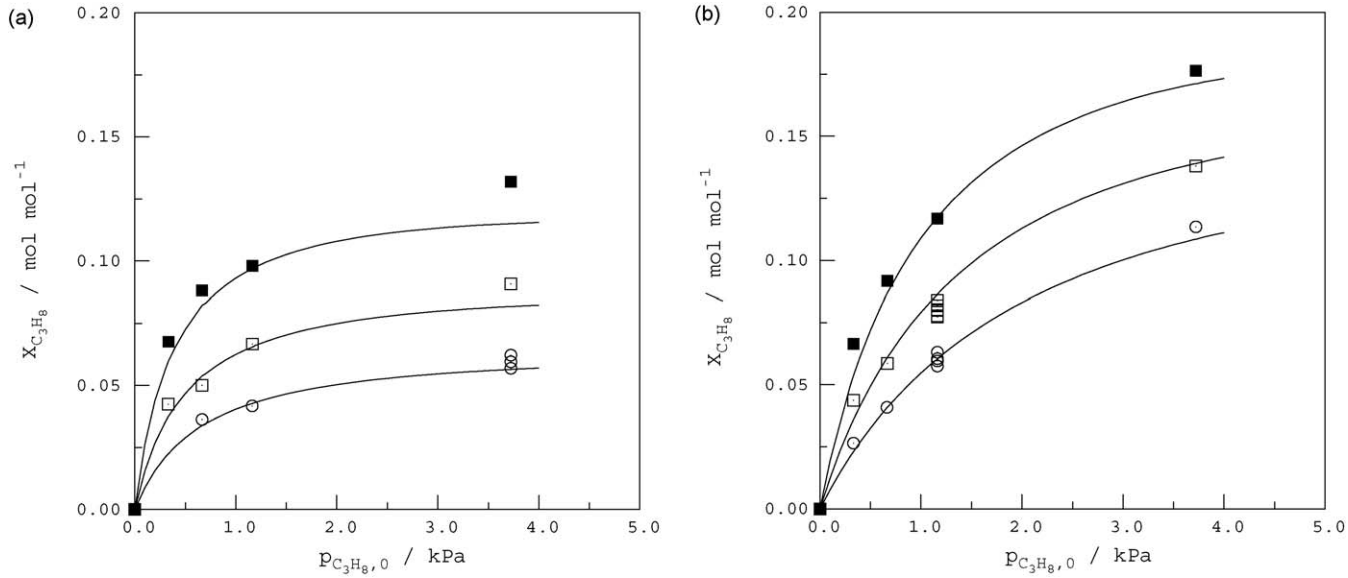

Fig. 3. Propane conversion vs. propane inlet partial pressure at $p_{O_2,0} = 28.4$ kPa and $W_{cat}F_{C_3H_8,0}^{-1} = 1970\ kg_{cat}\ s\ mol^{-1}$ on (a) Ti3-P and (b) Ti6-P. (○) 733 K; (□) 753 K; (■) 773 K. Full lines are obtained with model MVK1, reported in Table 6, and corresponding kinetic parameter values from Table 8.

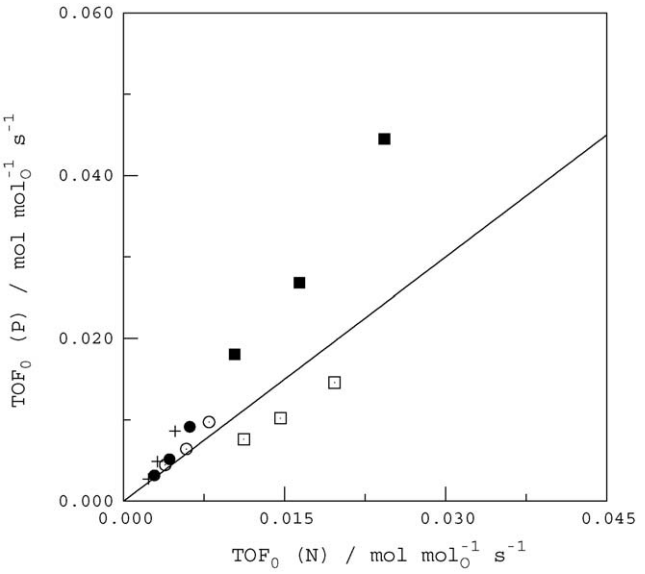

Fig. 4. Initial TOF obtained on porous support vs. initial TOF obtained on non-porous support at $p_{C_3H_8,0} = 1.16$ kPa and $p_{O_2,0} = 28.4$ kPa. (○) Ti3; (□) Ti6; (+) V; (●) Ti3 V; (■) Ti6 V.

support. For sputter depositions V, Ti3V and Ti6V, it seems that the observed apparent activation energy for the total oxidation of propane decreases as the TiO_x sputter deposition time increases, using the porous support. Surprisingly, an opposite trend is seen for the non-porous support. Nevertheless, the observed apparent activation energy is generally lower than in the case where the porous support is used.

Based on the initial TOF analysis, it is concluded that the type of support as well as the TiO_x sputter deposition influence the catalytic activity.

Table 5
Observed apparent activation energies E_{app}^{obs} (kJ mol^{-1}) with their 95% confidence intervals, obtained by regression of the initial specific reaction rates at given propane and oxygen inlet partial pressures with Eq. (7).

Sputter deposition	Non-porous support	Porous support
Ti3	85.0 ± 5.8	91.5 ± 0.8
Ti6	66.2 ± 3.1	76.5 ± 5.5
V	84.4 ± 9.0	134.7 ± 1.6
Ti3V	89.3 ± 0.6	124.7 ± 7.7
Ti6V	100.5 ± 2.9	106.1 ± 9.1

5. Selection of a kinetic model based on elementary steps

Using the experimental data obtained on sample Ti6V-P, isothermal regression analysis for all ER kinetic models and the models MVK2 and MVK3 does not result in a distinct minimum of the objective function, vide Eq. (9). Therefore, these models are eliminated from the list in Table 6. The elimination of the ER models for the description of the experimental combustion data is in line with the findings of Choudhary and Desmukh [39]. On the other hand, a pronounced minimum is found for all LH models as well as for the MVK1 model, resulting in realistic isothermal kinetic parameters for all LH models and the MVK1 model. Arrhenius diagrams for the parameters in model LH1 and MVK1 are given in Fig. 5. It can be seen that the adsorption equilibrium coefficients for oxygen and propane are nearly constant in the investigated experimental temperature range. Similar diagrams are obtained for the models LH2, LH3 and LH4. From these Arrhenius diagrams initial guesses are obtained for the pre-exponential factors, activation energies and reaction enthalpies in the non-isothermal regression procedure.

A non-isothermal regression for the four LH models including all experimental data, obtained on sample Ti6V-P, did not lead to significant estimates for the adsorption parameters in any of the four LH models. Setting the propane and the oxygen adsorption enthalpy zero one after the other, corresponding to the lowest individual t value, still does not result in significant pre-exponential factors for the propane and oxygen adsorption equilibrium coefficients. The inlet molar fraction of propane is low enough to assume that no significant information about the temperature dependency of the adsorption process can be gathered from the present experimental data. For the oxygen adsorption equilibrium coefficient an analogous reasoning can be put forward, since the inlet partial pressure is kept constant. These conclusions could be expected from the Arrhenius diagram in Fig. 5a. Further elaboration of the models LH1,

Table 6
Overview of the kinetic models, applied to the experimental data on Ti6V-P. For the LH and ER models, the surface reaction is assumed to be rate determining.

	Model	Model assumptions	Rate equation
1	LH1	Molecular oxygen chemisorption One oxygen species involved	$r = k_s \frac{K_{O_2} K_{C_3H_8} p_{O_2} p_{C_3H_8}}{(1+K_{O_2} p_{O_2} + K_{C_3H_8} p_{C_3H_8})^2}$
2	LH2	Molecular oxygen chemisorption Two oxygen species involved	$r = k_s \frac{K_{O_2}^2 K_{C_3H_8} p_{O_2}^2 p_{C_3H_8}}{(1+K_{O_2} p_{O_2} + K_{C_3H_8} p_{C_3H_8})^3}$
3	LH3	Oxygen chemisorbs dissociatively One oxygen species involved	$r = k_s \frac{\sqrt{K_{O_2}} K_{C_3H_8} \sqrt{p_{O_2}} p_{C_3H_8}}{(1+\sqrt{K_{O_2} p_{O_2}} + K_{C_3H_8} p_{C_3H_8})^2}$
4	LH4	Oxygen chemisorbs dissociatively Two oxygen species involved	$r = k_s \frac{K_{O_2} K_{C_3H_8} p_{O_2} p_{C_3H_8}}{(1+\sqrt{K_{O_2} p_{O_2}} + K_{C_3H_8} p_{C_3H_8})^3}$
5	ER1	Molecular oxygen chemisorption One oxygen species involved	$r = k_s \frac{K_{O_2} p_{O_2} p_{C_3H_8}}{1+K_{O_2} p_{O_2}}$
6	ER2	Molecular oxygen chemisorption Two oxygen species involved	$r = k_s \frac{K_{O_2}^2 p_{O_2}^2 p_{C_3H_8}}{(1+K_{O_2} p_{O_2})^2}$
7	ER3	Oxygen chemisorbs dissociatively One oxygen species involved	$r = k_s \frac{\sqrt{K_{O_2} p_{O_2}} p_{C_3H_8}}{1+\sqrt{K_{O_2} p_{O_2}}}$
8	ER4	Oxygen chemisorbs dissociatively Two oxygen species involved	$r = k_s \frac{K_{O_2} p_{O_2} p_{C_3H_8}}{(1+\sqrt{K_{O_2} p_{O_2}})^2}$
9	MVK1	Reduction and reoxidation step involves one active site	$r = \frac{k_{O_2} k_{C_3H_8} p_{O_2} p_{C_3H_8}}{k_{O_2} p_{O_2} + 5 k_{C_3H_8} p_{C_3H_8}}$
10	MVK2	Reduction step involves two oxidized surface sites	$r = \frac{k_{O_2} p_{O_2}}{5}\left[1+\varphi-\sqrt{2\varphi+\varphi^2}\right]\ \varphi = \frac{2k_{O_2} p_{O_2}}{5k_{C_3H_8} p_{C_3H_8}}$
11	MVK3	Reoxidation step involves two reduced surface sites	$r = k_{C_3H_8} p_{C_3H_8}\left[1+\varphi'-\sqrt{2\varphi'+\varphi'^2}\right]\ \varphi' = \frac{5k_{C_3H_8} p_{C_3H_8}}{2k_{O_2} p_{O_2}}$

LH2 and LH4 gives a significant negative pre-exponential factor for oxygen adsorption and a pre-exponential factor for propane adsorption, which is not significantly different from zero. Model LH3 results in pre-exponential factors for oxygen and propane adsorption, which are not significantly different from zero. The latter parameter has the lowest individual t value, and hence, it is set to zero. This is also done in models LH1, LH2 and LH4. These reduced LH models physically correspond with the surface reaction between chemisorbed oxygen and propane for a negligible propane fractional coverage. Non-isothermal regression for the reduced models LH1 and LH3 results in a non significant oxygen adsorption parameter, and hence, these models can be reduced to power law rate expressions PL1 and PL2, given by (12) and (13), respectively.

$$r = k'_s p_{O_2} p_{C_3H_8} \quad (12)$$

$$r = k''_s \sqrt{p_{O_2}}\, p_{C_3H_8} \quad (13)$$

For models LH2 and LH4 a significant negative oxygen adsorption parameter is obtained, which is physically not possible, and hence, these models are removed from the list. The elimination of the LH models is in line with the findings of Juusola et al. [40] and Bampenrat et al. [16], examining the *o*-xylene oxidation over a V-based catalyst and the naphthalene oxidation over CeO_2–ZrO_2 mixed oxide catalysts.

The estimated values with their 95% confidence interval for the models PL1 and PL2 are gathered in Table 7. Both pre-exponential factors and activation energies can be estimated significantly. The activation energies for both models are nearly equal. Furthermore, the calculated *F* value amounts respectively to 395 and 322, indicating a good global significance of the regression for models PL1 and PL2.

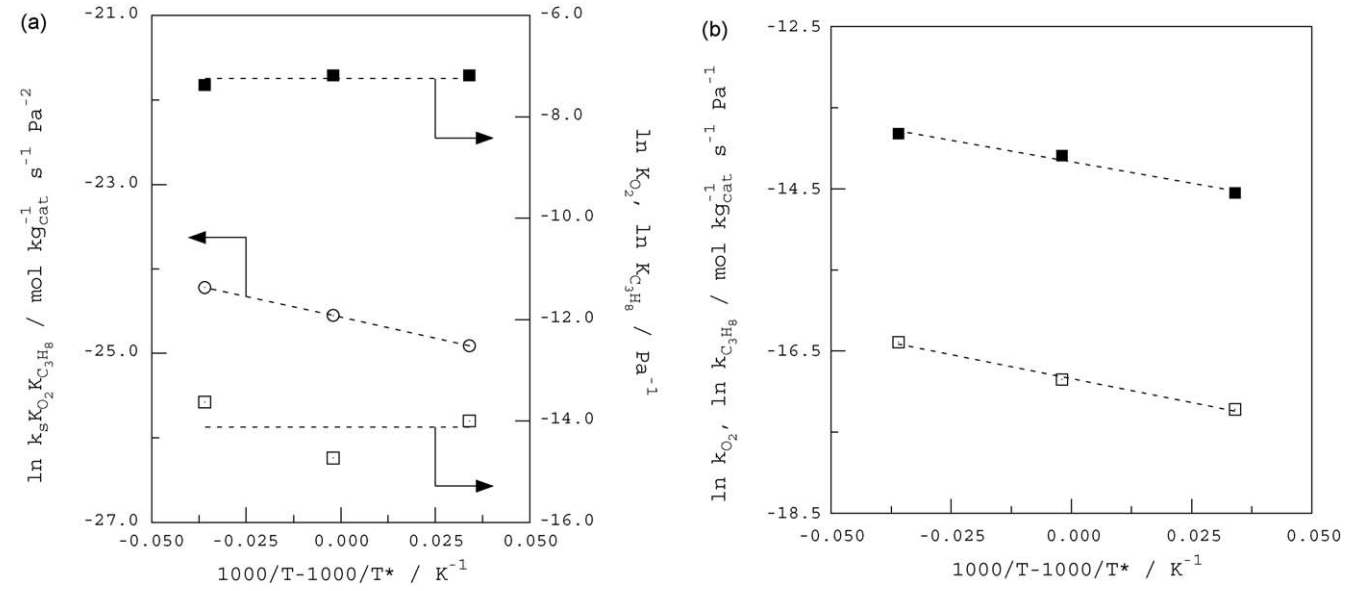

Fig. 5. Isothermal regression on sample Ti6V-P. (a) Model LH1: (○) $k_s K_{O_2} K_{C_3H_8}$; (□) K_{O_2}; (■) $K_{C_3H_8}$. (b) Model MVK1: (□) k_{O_2}; (■) $k_{C_3H_8}$. The models are reported in Table 6. The dashed lines are only shown to guide the eye.

Table 7
Estimates of pre-exponential factors and activation energies with their 95% confidence intervals obtained by regression of the experimental data on Ti6V-P for model PL1, using Eq. (12), model PL2, using Eq. (13) and model MVK1, using rate Eq. (9) given in Table 6. The corresponding residual sum of squares, vide Eq. (8), and the calculated F values are reported.

Model	Parameter	SI unit	Estimated value	RSSQ ($mol^2\ mol^{-2}$)	F_{calc}
PL1	$k'_{s,0}$	$\mu mol\ kg_{cat}^{-1}\ s^{-1}\ Pa^{-2}$	911.1 ± 20.3	0.039	395
	E'_s	$kJ\ mol^{-1}$	115.8 ± 4.1		
PL2	$k''_{s,0}$	$mmol\ kg_{cat}^{-1}\ s^{-1}\ Pa^{-3/2}$	118.7 ± 3.4	0.047	322
	E''_s	$kJ\ mol^{-1}$	114.4 ± 4.2		
MVK1	$k_{O_2,0}$	$mmol\ kg_{cat}^{-1}\ s^{-1}\ Pa^{-1}$	550.6 ± 93.8	0.011	605
	E_{O_2}	$kJ\ mol^{-1}$	101.5 ± 2.7		
	$k_{C_3H_8,0}$	$mmol\ kg_{cat}^{-1}\ s^{-1}\ Pa^{-1}$	295.3 ± 85.3		
	$E_{C_3H_8}$	$kJ\ mol^{-1}$	81.1 ± 4.6		

For the MVK1 model, all four kinetic parameters can be significantly estimated, vide Table 7. The pre-exponential factor for the reduction is a factor two lower than for the reoxidation and the activation energy for the latter is about 20.0 kJ mol^{-1} higher than the activation energy for reduction. Despite the higher pre-exponential factor, the rate coefficient for reoxidation is generally lower than the reduction rate coefficient. The F value for the global significance of the regression amounts to 605 indicating the good descriptive capabilities of the model. A maximum binary correlation coefficient between the pre-exponential factor for reoxidation and the activation energy for reduction of 0.91 is obtained, indicating that the estimated kinetic parameters are practically uncorrelated.

Application of the likelihood ratio as a selection criterion [22] between the models PL1, PL2 and MVK1 results in the selection of the latter model, which has the lowest residual sum of squares as well as the highest calculated F value.

This reduction–reoxidation mechanism is also observed in propane oxidative dehydrogenation on Cs-doped Cr-Mo-Al-O catalyst [18], the combustion of methyl isobutyl ketone over Pt/γ-Al_2O_3 catalyst [19], the catalytic incineration of $(CH_3)_2S_2$ over a $CuO–MoO_3/\gamma$-Al_2O_3 catalyst [41] and the propane and methyl ethyl ketone total oxidation over Cr-doped ZrO_2 catalyst respectively [39]. Oxidation experiments with $^{18}O_2$ clearly show that the total oxidation of propane over VO_x based catalysts occurs according to the MVK mechanism [42].

In Section 6, the selected MVK1 model is applied to the other nine experimental data sets in order to obtain kinetic parameters, which can be used for comparison amongst the different sputter deposited catalysts.

6. Mars–van Krevelen kinetic parameters for the investigated catalysts: estimation and assessment

The selected Mars–van Krevelen mechanism, MVK1, has been used to describe the experimental data on the other sputter deposited catalysts. The results of the non-isothermal parameter estimation procedure are listed in Table 8. The calculated F values for the experimental data on the other nine catalyst samples are higher than the value obtained on Ti6V-P. This indicates that the chosen model describes the experimental data on the other catalysts even better than on Ti6V-P and further justifies the selection of this mechanism.

From the Arrhenius diagrams constructed from the parameter values reported in Table 8, it can be observed that, taking into account all tested catalyst samples, the rate coefficients are reasonably concurrent, as shown in Fig. 6a for the reoxidation reaction. A similar result is obtained for the reduction rate coefficient. An increasing pre-exponential factor is accompanied by an increasing activation energy for the oxidation as well as for the reduction step, according to Eq. (14).

$$\ln k_0 = m_c E + b_c \tag{14}$$

This linear relation is known as 'compensation effect' [43,44]. Such an effect strictly holds for a series of slightly different catalysts using the same reactant [45]. Theoretical considerations have been made by Oudenhuijzen et al. [46] and Stepanov [47]. Although Bond [48] suggests that an observed compensation effect may be due to the presence of 'apparent' rather than 'true' Arrhenius parameters, the present results apply to 'real' Arrhenius parameters, i.e. those corresponding to a single elementary step.

The compensation effect for reduction and reoxidation separately on all the sputter deposited catalysts is visualized in Fig. 6b with a multiple correlation coefficient above 0.984, indicating the good fit according to Eq. (14). From the slope m_c the so-called 'isokinetic' temperature, T_{iso}, can be calculated from Eq. (15). At this temperature the reduction or reoxidation rate coefficient of all catalysts is identical [49,50].

$$T_{iso} = \frac{1}{m_c R} \tag{15}$$

Table 8
Parameter estimates with their 95% confidence intervals, obtained by non-isothermal regression of the experimental data with model MVK1, reported in Table 6. The average fraction of oxidized sites θ_{O^*} is obtained from Eq. (18).

Catalyst	F_{calc}	$k_{O_2,0}$ ($mol\ mol_O^{-1}\ s^{-1}\ Pa^{-1}$)	E_{O_2} ($kJ\ mol^{-1}$)	$k_{C_3H_8,0}$ ($mol\ mol_O^{-1}\ s^{-1}\ Pa^{-1}$)	$E_{C_3H_8}$ ($kJ\ mol^{-1}$)	θ_{O^*} [a]
Ti3-P	969	$(4.84 \pm 1.27) \times 10^{-1}$	78.9 ± 1.1	$(8.22 \pm 2.83) \times 10^{+4}$	139.2 ± 3.7	0.63 ± 0.39
Ti6-P	1014	$(6.04 \pm 0.81) \times 10^{-4}$	31.0 ± 1.5	$(1.62 \pm 0.24) \times 10^{+3}$	115.5 ± 1.8	0 [b]
V-P	2190	$(3.96 \pm 0.47) \times 10^{+4}$	150.9 ± 1.8	$(1.14 \pm 0.13) \times 10^{+0}$	73.1 ± 1.7	0.50 ± 0.13
Ti3V-P	1414	$(7.98 \pm 1.10) \times 10^{+4}$	155.6 ± 1.6	$(7.60 \pm 1.19) \times 10^{-3}$	40.1 ± 2.0	0.22 ± 0.02
Ti6V-P	605	$(5.01 \pm 0.85) \times 10^{+1}$	101.5 ± 2.7	$(2.69 \pm 0.78) \times 10^{+1}$	81.1 ± 4.6	0.23 ± 0.05
Ti3-N	2634	$(6.20 \pm 2.92) \times 10^{+0}$	94.4 ± 0.7	$(3.38 \pm 1.61) \times 10^{+0}$	79.5 ± 1.4	0.21 ± 0.02
Ti6-N	2291	$(2.02 \pm 0.32) \times 10^{-1}$	66.1 ± 1.2	$(6.33 \pm 1.03) \times 10^{+1}$	92.4 ± 1.4	0.54 ± 0.03
V-N	2072	$(5.54 \pm 0.84) \times 10^{-3}$	50.8 ± 1.4	$(7.23 \pm 1.06) \times 10^{+2}$	118.6 ± 1.3	0.21 ± 0.03
Ti3V-N	672	$(1.30 \pm 0.31) \times 10^{-1}$	69.8 ± 1.8	$(4.98 \pm 1.26) \times 10^{+5}$	158.5 ± 2.2	0.27 ± 0.07
Ti6V-N	1012	$(6.36 \pm 1.47) \times 10^{+2}$	117.8 ± 2.9	$(4.20 \pm 1.13) \times 10^{-2}$	43.8 ± 3.6	0 [b]

[a] Corresponding standard deviations are calculated from the 95% confidence intervals for the activation energies E_{O_2} and $E_{C_3H_8}$ and E_{app}^{obs} given in Table 5.
[b] Not significantly different from zero.

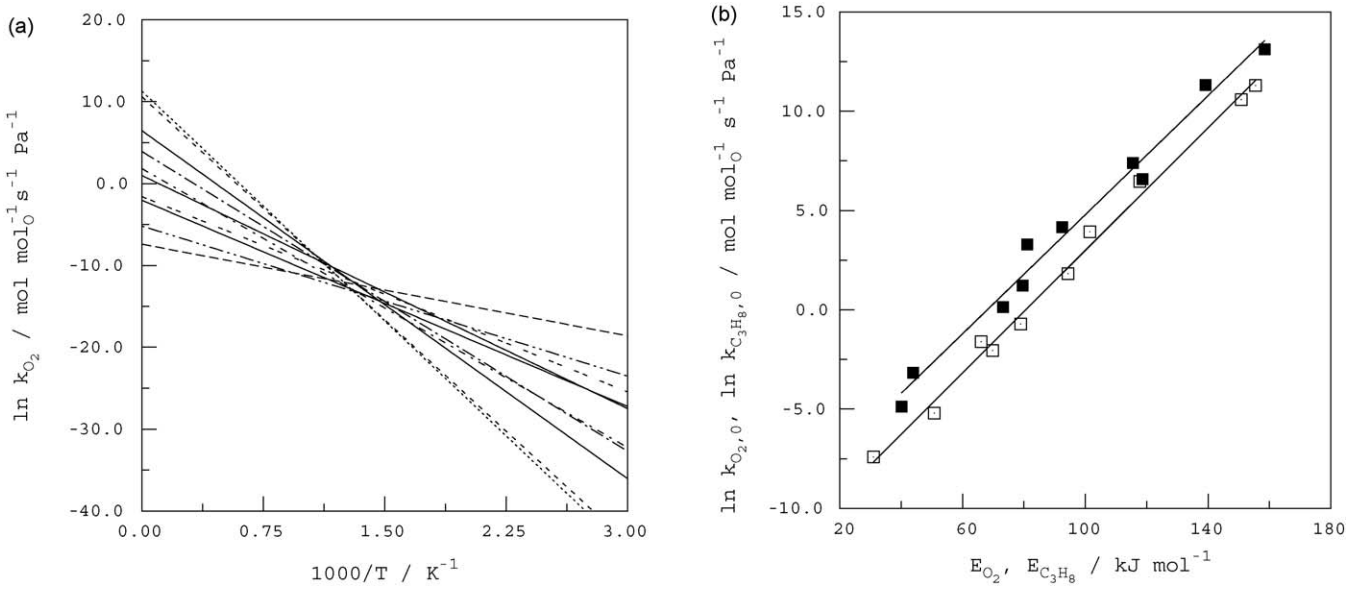

Fig. 6. (a) Logarithm of the oxidation rate coefficient vs. reciprocal of temperature. (····) Ti3-P; (—) Ti6-P; (– – –) V-P; (- - -) Ti3V-P; (· · ·) Ti6V-P; (–·–·–·) Ti3-N; (–·–·–·) Ti6-N; (– – –) V-N; (·–·–·) Ti3V-N; (— —) Ti6V-N. (b) Compensation effect for reduction and reoxidation. (□) Oxidation; (■) reduction. Full lines are obtained by linear regression of the kinetic data, taken from Table 8, with Eq. (14).

The isokinetic temperature for the reoxidation and reduction reaction amounts to 780 ± 2 K and 803 ± 4 K, respectively.

Secondly, from the observed apparent activation energies, E_{app}^{obs}, as determined from initial TOF analysis, vide Section 4, and the estimated activation energies for reoxidation and reduction, as reported in Table 8, an average for the fraction of oxidized and reduced sites can be determined. To that purpose, a theoretical apparent activation energy E_{app}^{calc} is calculated according to Eq. (16).

$$E_{app}^{calc} = RT^2 \frac{\partial \ln r}{\partial T} \tag{16}$$

When the rate expression for model MVK1, reported in Table 6, is used in Eq. (16), this results in a barycentric combination of the activation energies for oxidation and reduction, vide Eq. (17): the theoretical apparent activation energy equals the activation energy for oxidation when the catalyst surface is maximally reduced ($\theta_* = 1$) and for a maximally oxidized catalyst surface ($\theta_{O^*} = 1$) the theoretical apparent activation energy matches the activation energy for reduction.

$$E_{app}^{calc} = \theta_{O^*} E_{C_3H_8} + (1 - \theta_{O^*}) E_{O_2} \tag{17}$$

Setting the theoretical apparent activation energy E_{app}^{calc} equal to the observed apparent activation energy E_{app}^{obs}, vide Section 2.4, gives via Eq. (17) an average value for the fraction of oxidized sites θ_{O^*}, as given in Eq. (18).

$$\theta_{O^*} = \frac{E_{app}^{obs} - E_{O_2}}{E_{C_3H_8} - E_{O_2}} \tag{18}$$

From the observed apparent activation energies, summarized in Table 5, and the estimated activation energies for reoxidation and reduction, reported in Table 8, a reasonable average value for the fraction of oxidized sites can be obtained for all except two catalyst samples ranging from 0.21 ± 0.02 on Ti3-N to 0.63 ± 0.39 on Ti3-P. These values are given in Table 8.

The catalyst samples are also compared amongst each other based on their activity per active surface site or TOF. Distinctive features between the samples are the support, the sputter deposition time and the sputter deposited metal oxide. Using the parameter values in Table 8, the TOF is obtained for all catalyst samples using Eq. (9) from Table 6 at 0.20 mol mol^{-1} propane conversion and inlet pressures $p_{C_3H_8,0} = 1.16$ kPa and $p_{O_2,0} = 28.4$ kPa. Comparison based on an average value for the propane conversion is justified, because identical trends in TOF are observed for the whole propane conversion range. When Fig. 7a and b are inspected, no significant difference for the TOF corresponding to the samples V and Ti3V can be distinguished in the case of the porous support. For the non-porous support the initial TOF increases slightly, when Ti3V-N is compared to V–N. Further, a first TiO_x sputter deposition during 6 h results on both supports in a significantly higher TOF. In this case, it can be concluded that the sputter deposited TiO_x layer displays a more beneficial effect on the catalytic activity per V surface site than the actual support, since the TOF increases for an increasing TiO_x sputter deposition time. Further, it can be concluded that, despite the higher concentration of active sites present, mentioned in Table 1, the catalytic activity per active site is comparable for Ti6V-P and Ti6V-N over the whole temperature range.

The influence of the single TiO_x sputter deposition and the type of support is illustrated in Fig. 7c: the catalytic activity per surface site increases in the order Ti3-N ≤ Ti3-P < Ti6-*P* < Ti6-N. Apparently, above a certain TiO_x sputter deposition time, the non-porous (SiO_2–ZrO_2) support is energetically more beneficial than the porous (SiO_2) support. This observation is in line with the findings of Zaki et al. [51]. These authors use carbon monoxide oxidation over manganese supported oxides and observe an increase in catalytic activity according to the supports $ZrO_2 > Al_2O_3 > SiO_2$.

When the catalyst samples with a TiO_x sputter deposition time of three hours are looked at, vide Fig. 7a–c, the order of activity per surface site is Ti3V-N < Ti3V-P < Ti3-N ≈ Ti3-P. For a TiO_x sputter deposition time of 6 h the activity ranking reads: Ti6-P < Ti6-N < Ti6V-N ≈ Ti6V-P. This indicates that above a certain TiO_x sputter deposition time the VO_x sputter deposited samples become more active than the samples with only TiO_x. When the catalysts with a TiO_x sputter deposition time of 3 h are compared to the catalysts with a TiO_x sputter deposition time of 6 h, the corresponding TOF are globally higher.

The TOF at zero propane conversion, obtained with model MVK1, reported in Table 6, and kinetic parameters from Table 8, are in agreement with the initial TOF, experimentally determined

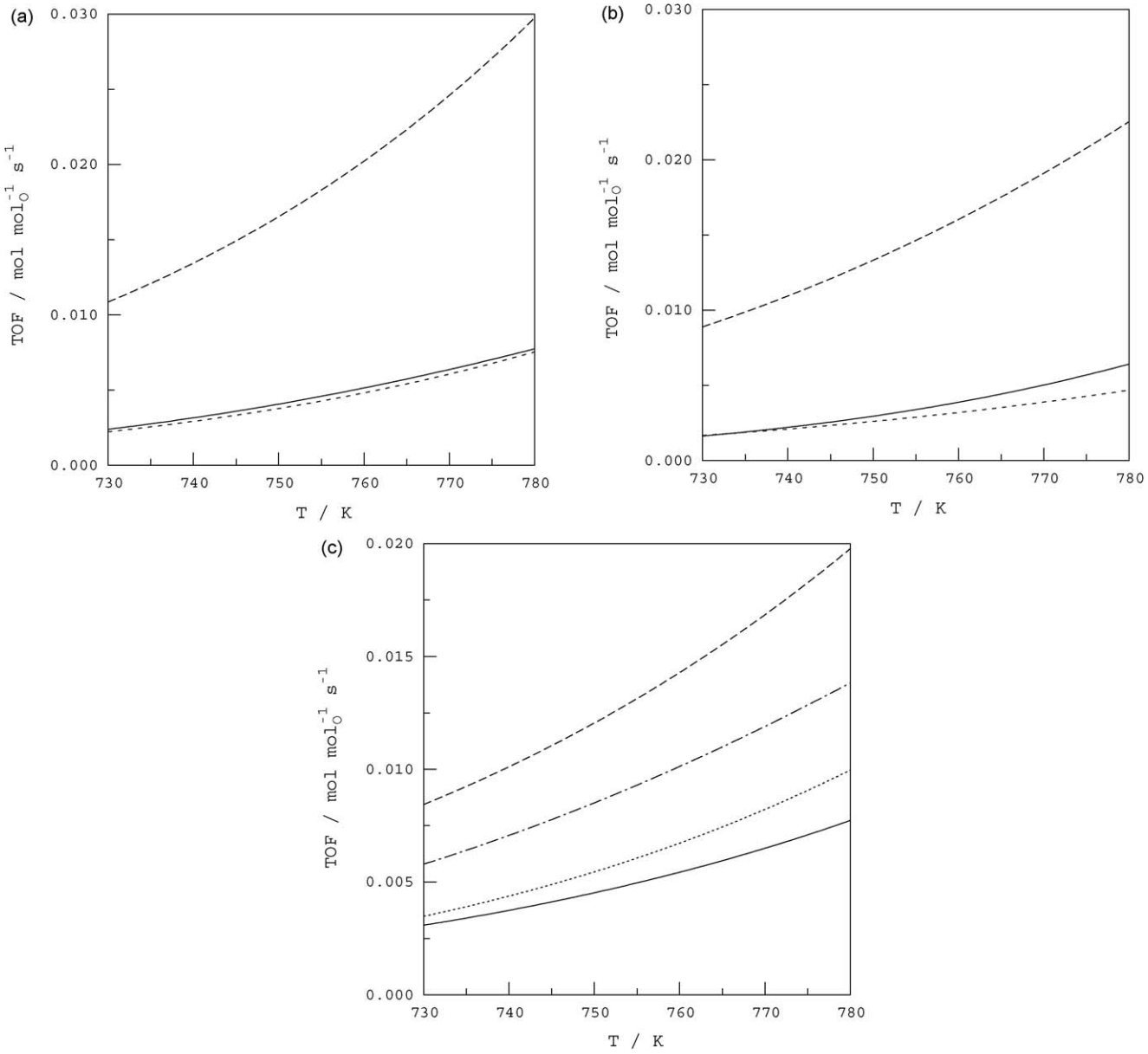

Fig. 7. TOF vs. temperature at $X_{C_3H_8} = 0.20\,\text{mol mol}^{-1}$, $p_{C_3H_8,0} = 1.16\,\text{kPa}$ and $p_{O_2,0} = 28.4\,\text{kPa}$. (a) VO_x sputter deposited samples on porous support. (····) V-P; (–) Ti3V-P; (– –) Ti6V-P. (b) VO_x sputter deposited samples on non-porous support. (····) V-N; (–) Ti3V-N; (—) Ti6V-N. (c) TiO_x sputter deposited samples. (–) Ti3-N; (——) Ti6-N; (····) Ti3-P; (–·–·–) Ti6-P. Lines are calculated with model MVK1, reported in Table 6, and corresponding kinetic parameter values from Table 8.

in Section 2.4: a maximal difference of 3.4 % is obtained, indicating that model based predictions correspond well with the experimental results acquired from Eqs. (4) and (5).

When the reaction coefficient for reduction and reoxidation are taken into account, the former is higher than the latter for all applied reaction temperatures. This is in accordance with the findings of Cellier et al. [52], pointing out that reoxidation in a MVK mechanism is the most difficult step in the reduction–reoxidation cycle. These results can be linked to the propane partial reaction order, which can be theoretically obtained according to Eq. (19).

$$n_{C_3H_8} = \left(\frac{\partial \ln r}{\partial \ln p_{C_3H_8}}\right)_{p_{O_2}} \tag{19}$$

Application of Eq. (19) to the MVK1 rate equation, given in Table 6, gives Eq. (20): for constant inlet conditions and propane conversion level, an increasing partial reaction order for propane is obtained with a decreasing ratio of rate coefficients for reduction and reoxidation.

$$n_{C_3H_8} = \frac{k_{O_2}(\gamma_0 - 5X_{C_3H_8})}{k_{O_2}(\gamma_0 - 5X_{C_3H_8}) + 5k_{C_3H_8}(1 - X_{C_3H_8})} \tag{20}$$

From Fig. 8 it is possible to rank the TiO_x sputter deposited catalyst samples according to the propane partial reaction order, namely Ti3-P < Ti3-N < Ti6-N < Ti6-P, which explains the propane inlet partial pressure dependency for Ti3-P and Ti6-P in Fig. 3.

The expression for propane partial reaction order, vide Eq. (20), equals formally the fraction of oxidized sites θ_{O^*} [21]. For identical inlet conditions and propane conversion level, the reduction degree increases when the ratio of rate coefficients for reduction and reoxidation increases, and hence, the origin of the above-mentioned average values for the fraction of oxidized sites obtained from Eq. (17), ranging from 0.21 ± 0.02 on Ti3-N to 0.63 ± 0.39 on Ti3-P, is elucidated.

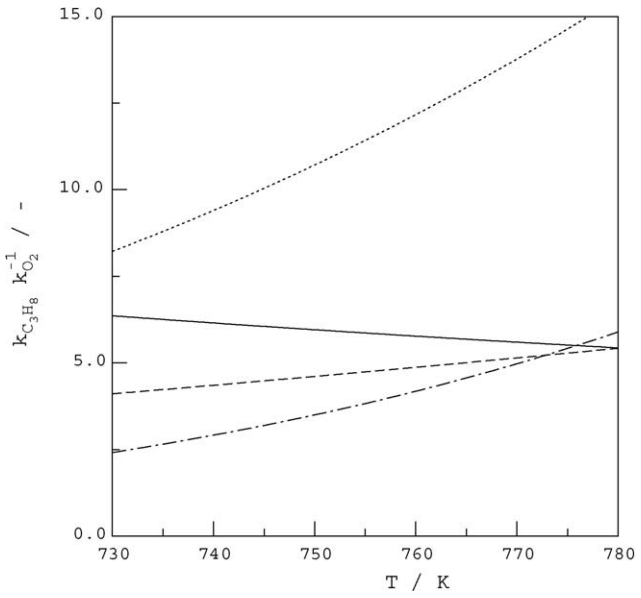

Fig. 8. Ratio of reduction and reoxidation rate coefficients vs. temperature. (–) Ti3-N; (——) Ti6-N; (····) Ti3-P; (-·–·–·) Ti6-P. Lines are calculated with model MVK1, reported in Table 6, and corresponding kinetic parameter values from Table 8.

7. Conclusions

The kinetics of the total oxidation of propane by sputter deposited vanadia–titania (anatase) based catalysts can be described most adequately by a Mars–van Krevelen reaction rate equation. The latter considers explicitly the reduction and the reoxidation of the catalyst. A statistically justified estimation of the kinetic parameters allows comparison amongst the tested catalyst samples based on calculated TOF over a wide range of experimental conditions. Catalyst preparation procedures such as used support, sputter deposition time and sputter deposited material are linked to TOF and rate coefficients for reduction and oxidation. A longer TiO_x sputter deposition time has a beneficial effect on the TOF. Furthermore, the use of a porous support results in higher initial TOF than when a non-porous support is applied. The estimated pre-exponential factor and activation energy for the reduction as well as the reoxidation show a clear compensation effect for the examined sputter deposited catalysts. Catalyst sample Ti6V-P has the highest specific catalytic activity as well as the highest activity per surface site, and hence, it is the most promising for total oxidation reactions.

Acknowledgements

This work was performed in the framework of a Concerted Research Action (GOA), financed by Ghent University. This work has also partly been performed within the IAP-PAI framework sponsored by the Belgian Science Policy.

References

[1] J.J. Spivey, Ind. Eng. Chem. Res. 26 (1987) 2165–2180.
[2] M. Zimowska, A. Michalik-Zym, R. Janik, T. Machej, J. Gurgul, R.P. Socha, J. Podobinski, E.M. Serwicka, Catal. Today 119 (2007) 321–326.
[3] M. Olea, I. Sack, V. Balcaen, G.B. Marin, H. Poelman, K. Eufinger, D. Poelman, R. De Gryse, J.S. Paul, B.F. Sels, P.A. Jacobs, Appl. Catal. A: Gen. 318 (2007) 37–44.
[4] H. Poelman, K. Eufinger, D. Depla, D. Poelman, R. De Gryse, B.F. Sels, G.B. Marin, Appl. Catal. A: Gen. 325 (2007) 213–219.
[5] H. Poelman, B.F. Sels, M. Olea, K. Eufinger, J.S. Paul, B. Moens, I. Sack, V. Balcaen, F. Bertinchamps, E.M. Gaigneaux, P.A. Jacobs, G.B. Marin, D. Poelman, R. De Gryse, J. Catal. 245 (2007) 156–172.
[6] I. Safi, Surf. Coat. Technol. 127 (2000) 203–219.
[7] H. Tomaszewski, H. Poelman, D. Depla, D. Poelman, R. De Gryse, L. Fiermans, M.F. Reyniers, G. Heynderickx, G.B. Marin, Vacuum 68 (2002) 31–38.
[8] S. Brunauer, P.H. Emmett, E. Teller, J. Am. Chem. Soc. 60 (1938) 309–319.
[9] P. Malet, A. Caballero, J. Chem. Soc. Faraday Trans. 84 (1988) 2369–2375.
[10] F. Kapteijn, J.A. Moulijn, A. Tarfaoui, in: J.A. Moulijn, P.W.N.M. van Leeuwen, R.A. van Santen (Eds.), Catalysis: An Integrated Approach to Homogeneous, Heterogeneous and Industrial Catalysis, Elsevier, Amsterdam, 1993, pp. 401–417.
[11] G. Centi, S. Perathoner, Int. J. Mol. Sci. 2 (2001) 183–196.
[12] T. Garcia, B. Solsona, D.M. Murphy, K.L. Antcliff, S.H. Taylor, J. Catal. 229 (2005) 1–11.
[13] V. Murgia, E. Sham, J.C. Gottifredi, E.M.F. Torres, Lat. Am. Appl. Res. 34 (2004) 75–82.
[14] R.J. Berger, E.H. Stitt, G.B. Marin, F. Kapteijn, J.A. Moulijn, Cattech 5 (2001) 30–60.
[15] D. Klvana, J. Vaillancourt, J. Kirchnerova, J. Chaouki, Appl. Catal. A: Gen. 109 (1994) 181–193.
[16] A. Bampenrat, V. Meeyoo, B. Kitiyanan, P. Rangsunvigit, T. Rirksomboon, Catal. Commun. 9 (2008) 2349–2352.
[17] L.Y. Hsu, H.S. Teng, Appl. Catal. B: Environ. 35 (2001) 21–30.
[18] B.Y. Jibril, S.M. Al-Zahrani, A.E. Abasaeed, R. Hughes, Chem. Eng. J. 103 (2004) 59–67.
[19] T.K. Tseng, H. Chu, T.H. Ko, L.K. Chaung, Chemosphere 61 (2005) 469–477.
[20] R. Burch, D.J. Crittle, M.J. Hayes, Catal. Today 47 (1999) 229–234.
[21] M.A. Vannice, Kinetics of Catalytic Reactions, Springer, New York, 2005.
[22] G.F. Froment, L.H. Hosten, in: J.R. Anderson, M. Boudart (Eds.), Catalysis Science and Technology, Springer-Verlag, Berlin, 1981, pp. 97–170.
[23] D.M. Espie, S. Macchietto, Ind. Eng. Chem. Res. 27 (1988) 2175–2179.
[24] D.M. Himmelblau, Process Analysis by Statistical Methods, Wiley, New York, 1970.
[25] G. Ertl, H. Knözinger, J. Weitkamp, Preparation of Solid Catalysts, Wiley-VCH, Weinheim, 1999.
[26] J.A. Moulijn, A.E. van Diepen, F. Kapteijn, Appl. Catal. A: Gen. 212 (2001) 3–16.
[27] H. Bosch, B.J. Kip, J.G. Vanommen, P.J. Gellings, J. Chem. Soc. Faraday Trans. 80 (1984) 2479–2488.
[28] T. Machold, W.Y. Suprun, H. Papp, J. Mol. Catal. A: Chem. 280 (2008) 122–130.
[29] B. Moden, L. Oliviero, J. Dakka, J.G. Santiesteban, E. Iglesia, J. Phys. Chem. B 108 (2004) 5552–5563.
[30] K.V.R. Chary, J. Chem. Soc. Chem. Commun. (1989) 104–105.
[31] K.V.R. Chary, K. Narsimha, K.S.R. Rao, B.R. Rao, P.K. Rao, J. Mol. Catal. 58 (1990) L13–L17.
[32] M. Kobayashi, B. Golman, T. Kanno, S. Fujisaki, Appl. Catal. A: Gen. 151 (1997) 193–205.
[33] F. Majunke, M. Baerns, A. Baiker, R.A. Koeppel, Catal. Today 20 (1994) 53–59.
[34] S.T. Oyama, G.T. Went, K.B. Lewis, A.T. Bell, G.A. Somorjai, J. Phys. Chem. 93 (1989) 6786–6790.
[35] C.H. Bamford, C.F.H. Tipper, Complex Catalytic Processes, Elsevier Scientific Pub. Co, Amsterdam, 1978.
[36] S.T. Oyama, A.N. Desikan, J.W. Hightower, Catal. Selective Oxid. 523 (1993) 1–14.
[37] S.T. Oyama, A.N. Desikan, W. Zhang, Catal. Selective Oxid. 523 (1993) 16–30.
[38] J.M. Herrmann, Catal. Today 112 (2006) 73–77.
[39] V.R. Choudhary, G.M. Deshmukh, Chem. Eng. Sci. 60 (2005) 1575–1581.
[40] J.A. Juusola, R.F. Mann, J. Downie, J. Catal. 17 (1970) 106–113.
[41] C.H. Wang, S.S. Lin, H.S. Weng, J. Environ. Sci. Health.A: Toxic/Hazard. Subst. Environ. Eng. 37 (2002) 1649–1663.
[42] K. Scheurell, E. Hoppe, K.W. Brzezinka, E. Kemnitz, J. Mater. Chem. 14 (2004) 2560–2568.
[43] A.K. Galwey, D.G. Bettany, M. Mortimer, Int. J. Chem. Kinet. 38 (2006) 689–702.
[44] J.J. Rooney, J. Mol. Catal. A: Chem. 133 (1998) 303–305.
[45] R. Larsson, Catal. Today 1 (1987) 93–99.
[46] M.K. Oudenhuijzen, J.A. van Bokhoven, D.C. Koningsberger, J. Catal. 219 (2003) 134–145.
[47] I.A. Stepanov, Monatsh. Chem. 128 (1997) 837–839.
[48] G.C. Bond, Catal. Today 49 (1999) 41–48.
[49] K.M. Bratlie, Y.M. Li, R. Larsson, G.A. Somorjai, Catal. Lett. 121 (2008) 173–178.
[50] O. Exner, Nature 227 (1970) 366–367.
[51] M. Zaki, M.A. Hasan, L. Pasupulety, N.E. Fouad, H. Knozinger, New J. Chem. 23 (1999) 1197–1202.
[52] C. Cellier, V. Ruaux, C. Lahousse, P. Grange, E.M. Gaigneaux, Catal. Today 117 (2006) 350–355.
[53] R.J. Berger, J. Perez-Ramirez, F. Kapteijn, J.A. Moulijn, Chem. Eng. Sci. 57 (2002) 4921–4932.
[54] H. Gierman, Appl. Catal. 43 (1988) 277–286.
[55] D.E. Mears, Chem. Eng. Sci. 26 (1971) 1361–1366.